Formation of Forward and Reverse Shock Waves in a Magnetized Plasma: Two-Dimensional Particle Simulations*)

Tatsunori URAGAMI and Mieko TOIDA

Department of Physics, Nagoya University, Nagoya 464-8602, Japan

(Received 19 November 2012 / Accepted 9 September 2013)

Interactions of exploding and surrounding plasmas are studied with two-dimensional (2D) electromagnetic particle simulations, for a case in which the initial velocity of the exploding plasma is perpendicular to an external magnetic field. It is confirmed that essentially the same phenomena (the penetration of exploding ions, the formation of a strong magnetic-field pulse, and the generation of forward and reverse shock waves) as in the previous one-dimensional (1D) simulations occurred in the 2D simulation. Further, modified two-stream instabilities excited by relative cross-field motion between ions and electrons are investigated with attention to their effects on the 2D structure of the strong magnetic-field pulse and on ion reflection by the pulse.

Keywords: collisionless shock, modified two-stream instability, whistler wave, particle simulation

DOI: 10.1585/pfr.8.2401155

1. Introduction

Shock waves can be generated from strong disturbances, such as solar flares and supernova explosions, and are believed to play an essential role in producing high energy particles. Particle simulations have demonstrated that a large-amplitude magnetosonic shock wave can accelerate ions, electrons, and positrons through various nonstochastic mechanisms caused by strong electromagnetic fields near a shock front [1, 2]. These studies were concerned with acceleration processes after formation of a shock wave.

Shock formation process from a strong disturbance in a collisionless plasma has also been an important issue in plasma physics [3, 4] because it would be quite different from that in collisional fluids. In Ref. [5], interactions of two plasmas, surrounding and exploding plasmas, and resultant generation of large-amplitude waves in an external magnetic field have been investigated with theories and simulations. It has been shown that a strong magnetic-field pulse is produced near the initial boundary of the two plasmas, from which the forward and reverse shock waves are created. Furthermore, the generation of large-amplitude Alfven waves and acceleration of electrons in these waves [6] have been reported. These theories and simulations [5,6] are concerned with one-dimensional (1D) effects, and multidimensional effects on the wave evolution have not been investigated.

In this study, by using two-dimensional (2D) electromagnetic particle simulations, we investigate the interactions of exploding and surrounding plasmas for a case in which the initial velocity of the exploding plasma $\boldsymbol{v}_0$ is perpendicular to the external magnetic field $\boldsymbol{B}_0$. After describing the simulation model and parameters in sec. 2, we verify the previous 1D result [5] with the 2D simulation in sec. 3. We confirm the theoretical predictions for plasma motions and show that forward and reverse shock waves are created after the formation of a strong magnetic-field pulse. In sec. 4, we study the 2D structure due to modified two-stream instabilities excited by relative cross-field motion between ions and electrons through interaction with whistler waves. Multidimensional effects on ion reflection by the strong magnetic-field pulse are also discussed.

2. Simulation Model and Parameters

We use a 2D (two spatial coordinates and three velocity components) relativistic electromagnetic particle code with full ion and electron dynamics to study the interactions of exploding and surrounding plasmas and the resultant formation of shock waves. A uniform external magnetic field is in the z direction $\boldsymbol{B}_0 = (0, 0, B_{z0})$, and the simulation plane is (x, z) with a size $L_x \times L_z = 8192\Delta_g \times 512\Delta_g$, where Δ_g is the grid spacing. The total number of simulation particles is $N \simeq 1.1 \times 10^9$.

At $t = 0$, we have an exploding plasma with a fluid velocity $\boldsymbol{v}_0 = (v_0, 0, 0)$ in the region $x < b$ and a surrounding plasma at rest in the region $x > b$. The values of b and v_0 are set to be $b = 3300\Delta_g$ and $v_0 = 12v_A$. The initial density ratio of exploding to surrounding plasmas is $n_{E0}/n_{S0} = 2$. The ion-to-electron mass ratio is $m_i/m_e = 200$. The light speed is $c/(\omega_{pe}\Delta_g) = 4.0$, and the electron and ion thermal velocities in the upstream region are $v_{Te}/(\omega_{pe}\Delta_g) = 0.5$ and $v_{Ti}/(\omega_{pe}\Delta_g) = 0.035$, respectively, where ω_{pe} is the electron plasma frequency averaged over the entire region. The magnetic field strength is $|\Omega_e|/\omega_{pe} = 0.5$; hence, the

author's e-mail: toida@cc.nagoya-u.ac.jp

*) This article is based on the presentation at the 22nd International Toki Conference (ITC22).

Alfven speed is $v_A/(\omega_{pe}\Delta_g) = 0.14$.

3. Evolution of 1D Averaged Quantities

In this section, we compare the 2D simulation results with the previous 1D theories and simulations. A theory of characteristic curves for plasma motions is presented in Ref. [5], where the effects of E_y induced by the cross field-motion of exploding ions are analyzed for the time scale $|\Omega_e|^{-1} < t \lesssim |\Omega_i|^{-1}$, where Ω_e and Ω_i are electron and ion gyro-frequencies, respectively. It is shown that the trajectories of particles that are initially at the boundary $x = b$ are written as

$$x_{iEb} = v_d t - (v_0 - v_d)\sin(-\Omega_i t)/\Omega_i + b, \quad (1)$$

$$x_{iSb} = v_d t + v_d(1 + r_{xy}^2/2)\sin(-\Omega_i t - r_{xy})/\Omega_i + b + v_d r_{xy}/\Omega_i, \quad (2)$$

$$x_{eb} = v_d t + b, \quad (3)$$

with $v_d = cE_y/B_z$ and $r_{xy} = E_x/E_y$. Here, x_{iEb} and x_{iSb} are for exploding and surrounding ions, respectively. As for electrons, the two kinds of electrons, which are initially separated in the coordinate space, will not mixed up later if the drift approximation is valid. This boundary is denoted by x_{eb}.

The upper panel in Fig. 1 shows the theoretical characteristic curves given by eqs. (1)-(3), for which we have set $E_y/B_{z0} = 0.25$, $r_{xy} = 0.1$ (these values are consistent with the simulation result), and $\Omega_i = \Omega_{i0}$, which is calculated using the external magnetic field strength. In the early phase, x_{iEb} moves faster than x_{iSb}, indicating that the exploding ions penetrate in the surrounding plasma, and the exploding and surrounding ions overlap in the region $x_{iSb} < x < x_{iEb}$. The electric field E_y induced by the cross-field motion of exploding ions quickly accelerates the surrounding ions in the y direction. Because of $\boldsymbol{v} \times \boldsymbol{B}$ force, v_y of the surrounding ions is converted to v_x, and v_x of the exploding ions is converted to v_y. As a result, the two characteristic curves x_{iSb} and x_{iEb} subsequently intersect again.

The lower panel in Fig. 1 shows the trajectories of 2D simulation particles; we followed the orbits of particles that were initially in the regions $b - \Delta_g < x < b$ and $b < x < b + \Delta_g$ for exploding and surrounding plasmas, respectively, and plotted their averaged orbits. A comparison of the two panels in Fig. 1 shows that the trajectories of 2D simulation particles can be explained by eqs. (1)-(3), although the time and space scales in the lower panel are different from those in the upper panel; this is because the 2D simulation particles experience the magnetic field that is gradually intensified, which is not considered in the theory.

We now consider the evolution of magnetic field B_z averaged along the z direction, $\bar{B}_z$. Figure 2 shows $\bar{B}_z$ as a function of x and t, where x_{iSb}, x_{iEb}, and x_{eb} are the same as in the lower panel in Fig. 1. In the early stage, $\Omega_{i0}t < 1$, $\bar{B}_z$ is intensified in the region $x_{eb} < x < x_{iEb}$, and a strong magnetic-field pulse is formed. At $\Omega_{i0}t \simeq 1$, the pulse splits into two pulses, which then develop into shock waves, one going forward and the other backward. This is caused by the ion reflection. The surrounding (exploding) ions are reflected forward (backward), which produces the forward (reverse) shock wave. The ion phase-space plots will be discussed later.

It is thus confirmed that essentially the same phenomena in the 1D simulation (the penetration of exploding ions, overtaking of surrounding ions, intensification of the magnetic field, and formation of two pulses) have been observed in the 2D simulation.

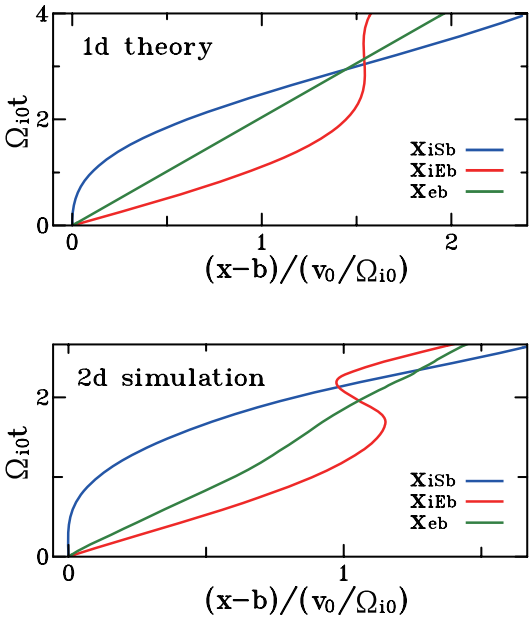

Fig. 1 Characteristic curves for ions and electrons that are initially at the boundary of exploding and surrounding plasmas. The upper panel shows the theoretical curves (1), (2), and (3), and the lower panel displays the trajectories of 2D simulation particles.

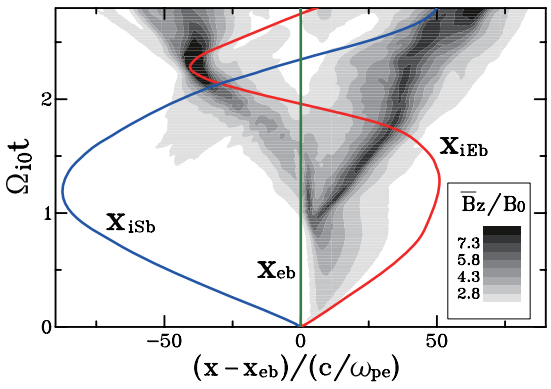

Fig. 2 Evolution of z-averaged magnetic field $\bar{B}_z(x, t)$.

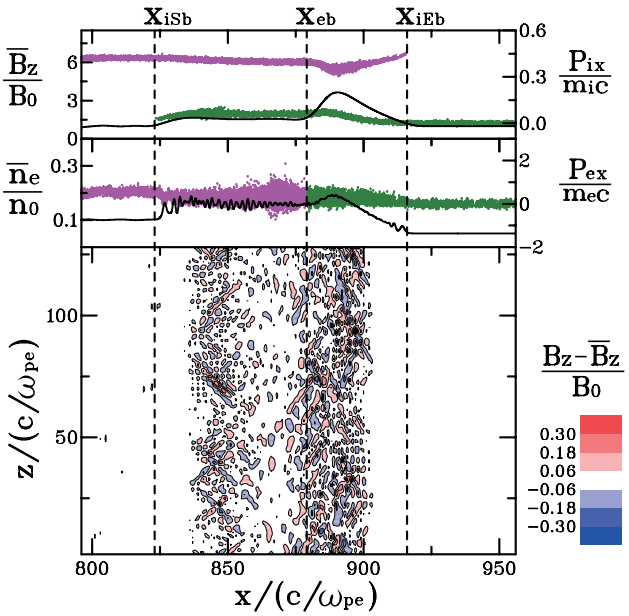

Fig. 3 Profiles of z-averaged B_z and n_e, contour map of 2D fluctuation of B_z, and ion and electron phase-space plots (x, p_x) at $\Omega_{i0}t = 0.55$. Pink and green dots represent exploding and surrounding particles, respectively.

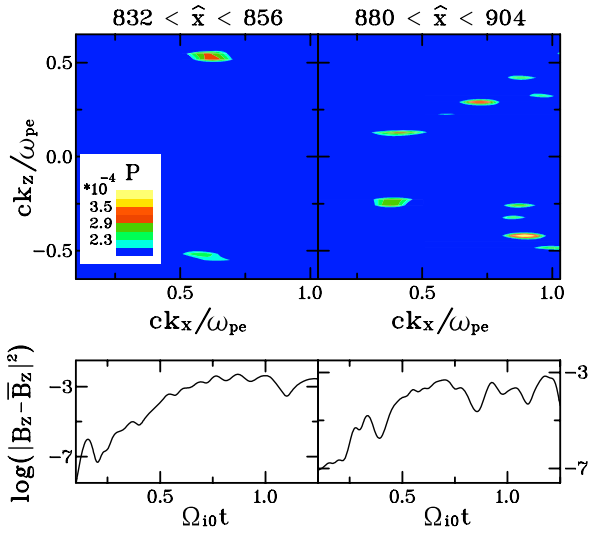

Fig. 4 Power spectra, $P(k_x, k_z)$, of B_z in the left- and right-hand sides of x_{eb} at $\Omega_{i0}t = 0.55$ and time variation of the amplitudes of the dominant modes.

4. Multi-Dimensional Structure

Relative cross-field motion between ions and electrons in the ion-overlapping region $x_{iSb} < x < x_{iEb}$ can excite modified two-stream instabilities through interaction of whistler waves [7, 8], which are not included in 1D simulations. We study the evolution of the instabilities in the magnetic field being gradually compressed because of a collision of two plasmas.

Figure 3 displays the x profiles of z-averaged B_z and electron density n_e, ion and electron phase-space plots (x, p_x), and the contour map of $B_z - \bar{B}_z$ in the (x, z) plane at $\Omega_{i0}t = 0.55$; the pink and green dots are for the exploding and surrounding particles, respectively. The bottom panel shows that 2D fluctuations are excited in the region where the surrounding and exploding ions overlap.

The upper panel in Fig. 4 shows the power spectra $p(k_x, k_z)$ of the magnetic field in the regions $x_{iSb} < x < x_{eb}$ and $x_{eb} < x < x_{iEb}$ at $\Omega_{i0}t = 0.55$. These regions are the left- and right-hand sides of the electron boundary $x = x_{eb}$, respectively, which we call left and right regions. The wavenumber of the dominant mode in the left region is $(ck_x/\omega_{pe}, ck_z/\omega_{pe}) = (0.62, 0.53)$, which is different from that in the right region $(0.89, -0.42)$. This difference may be caused by the fact that the magnetic field in the right region is intensified, compared to that in the left region. The lower panel in Fig. 4 shows the time variations of the amplitudes of these dominant modes.

We compare the simulation results with a linear theory. We assume that ions are effectively unmagnetized while electrons are magnetized. Then, a linear dispersion relation for a system with two ion beams interacting with whistler modes is written, in the electron rest frame, as

$$\frac{\omega^2}{\Omega_e^2} - \frac{c^4k^4\cos^2\theta}{\omega_{pe}^4(1+c^2k^2/\omega_{pe}^2)^2} - \frac{\omega^2}{\omega_{pe}^2}\frac{c^2k^2/\omega_{pe}^2}{1+c^2k^2/\omega_{pe}^2}\left[\frac{\omega_{pa}^2}{(\omega-k_xV_{a0})^2} + \frac{\omega_{pb}^2}{(\omega-k_xV_{b0})^2}\right] = 0, \quad (4)$$

where the subscripts a and b denote two different ion groups (surrounding and exploding ions), and θ is the propagation angle of whistler modes. Equation (4) predicts that if $V_{a0} > V_{b0}$, waves excited by a-ions have greater growth rates than those by b-ions. The condition for the destabilization is

$$\theta < \theta_{max} = \arctan[(m_i/m_e)^{1/2}v_A/2V_{a0}]. \quad (5)$$

Because the magnetic field is intensified in the right region, θ_{max} for this region, 78°, is greater than that for the left region, 63°. We have estimated θ_{max} by substituting the observed values of magnetic field, plasma density, and ion speed in Eq. (5). The upper panel in Fig. 4 shows that the excited waves satisfy the condition (5). The value of θ of the dominant mode is 65° for the right region (49° for the left region). The theoretical growth rate of the dominant mode, which is calculated from Eq. (4), is $\gamma = 0.029|\Omega_e|$ for the right region ($0.034|\Omega_e|$ for the left region), which is close to the observed growth rate shown in the lower panel in Fig. 4, $\gamma = 0.022|\Omega_e|$ ($0.031|\Omega_e|$). From Eq. (4), we can estimate that θ and wavenumber k for the modes that have maximum growth rates are $\theta \simeq 69°$ and $ck/\omega_{pe} \simeq 1.7$ for the right region, and $\theta \simeq 48°$ and $ck/\omega_{pe} \simeq 2.0$ for the left region. These theoretical θ's of the most unstable modes are close to θ's of the dominant modes observed in the simulation. The observed wavenumbers are smaller

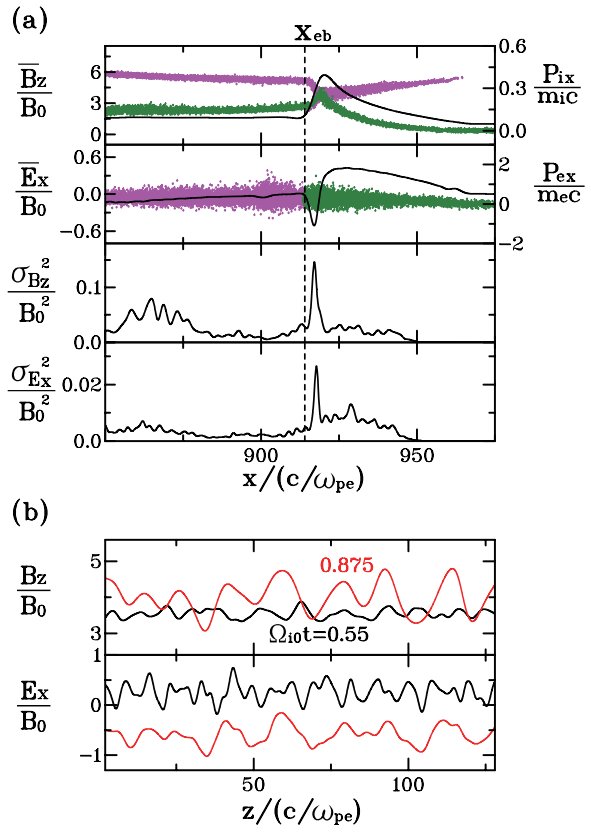

Fig. 5 (a) Profiles of $\bar{B}_z(x)$, $\bar{E}_x(x)$, and of the magnitudes of the 2D fluctuations of B_z and E_x defined by Eq. (6) at $\Omega_{i0}t = 0.875$. Electron and ion phase-space plots are also plotted. (b) Variations of B_z and E_x along z at fixed x positions where $\sigma^2_{B_z}$ and $\sigma^2_{E_x}$ become maximum, respectively.

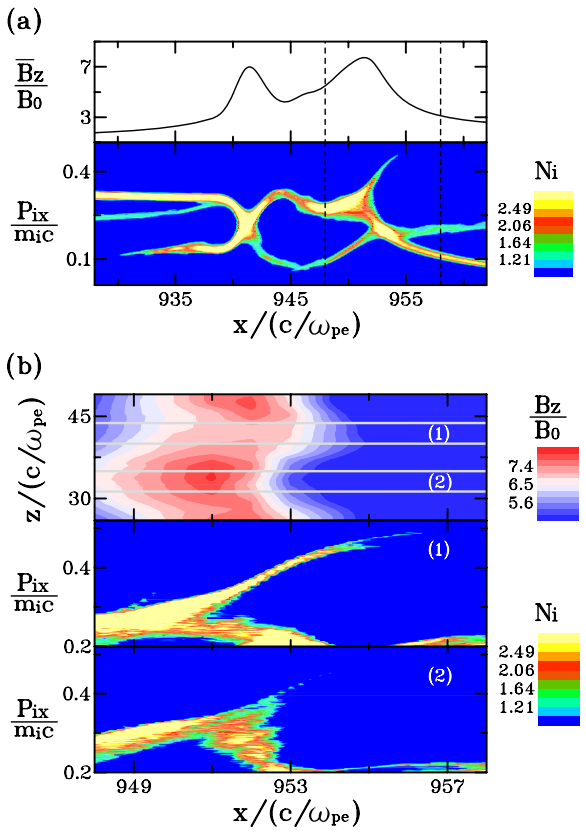

Fig. 6 (a) Profile of $\bar{B}_z$ and ion phase-space plot at $\Omega_{i0}t = 1.125$. (b) Expanded view of right-pulse region. Contour map of B_z in the (x, z) plane and ion distributions for different z ranges.

than the theoretical ones; the former is about 58% of the latter for the right region and 41% for the left region. This may be because as k increases, whistler waves approach electrostatic waves; at $\Omega_{i0}t \simeq 0$, amplitudes of magnetic fluctuations were quite small at the wavenumbers where the theoretical growth rate becomes maximum, compared to those at smaller wavenumbers. Because the modes with the smaller wavenumbers are also unstable, we observed, at $\Omega_{i0}t = 0.55$, large-amplitude magnetic fluctuations at these wavenumbers in the upper panel of Fig. 4.

We now study the nonlinear evolution of the instabilities. Figure 5 (a) shows the x profiles of z-averaged B_z and E_x and of the magnitudes of 2D fluctuations of B_z and E_x at $\Omega_{i0}t = 0.875$, where σ^2_F with $F = B_z$ or E_x is defined as

$$\sigma^2_F(x,t) = \frac{1}{L_z}\int_0^{L_z} dz[F(x,z,t) - \bar{F}(x,t)]^2, \qquad (6)$$

where $\bar{F}(x,t)$ is the z-averaged $F(x,z,t)$. We note that the magnitudes of the 2D fluctuations are noticeably great near the boundary of the exploding and surrounding electrons, $x = x_{eb}$, and near the positions where $\bar{B}_z$ has a strong slope. Figure 5 (b) shows the variations of B_z and E_x along the z direction; the values of B_z and E_x are at fixed x positions where $\sigma^2_{B_z}$ and $\sigma^2_{E_x}$ become maximum, respectively. For comparison, B_z and E_x at earlier time, $\Omega_{i0}t = 0.55$, are also plotted. The 2D fluctuations at later time ($\Omega_{i0}t \sim 0.875$) have longer wavelength and greater amplitudes. The mechanism for the intensification of 2D fluctuation with longer wavelengths near $x = x_{eb}$ is unclear, although it seems that this nonlinear development is caused by strong current flowing there.

At $\Omega_{i0}t = 0.95$, the strong magnetic-field pulse starts to reflect surrounding ions forward and exploding ions backward. Figure 6 (a) shows the profile of $\bar{B}_z$ and the ion phase space plot (x, p_x) at $\Omega_{i0}t = 1.125$, where the color indicates the ion number density including both the surrounding and exploding ions. Because the ion reflection has already started, there are two pulses in Fig. 6 (a). The ions in front of the right pulse [$952 < x/(c/\omega_{pe}) < 955$] with $p_{ix} > 0.3m_ic$ are reflected surrounding ions, and the ions behind the left pulse [$930 < x/(c/\omega_{pe}) < 940$] with $p_{ix} < 0.2m_ic$ are the reflected exploding ions. The strength of ion reflection depends on the position z because the electromagnetic fields vary along z direction, as shown in Fig. 5. Figure 6 (b) displays the expanded view of the right pulse region. The upper panel shows the contour map of B_z in the (x, z) plane for the small regions $948 < x/(c/\omega_{pe}) <$

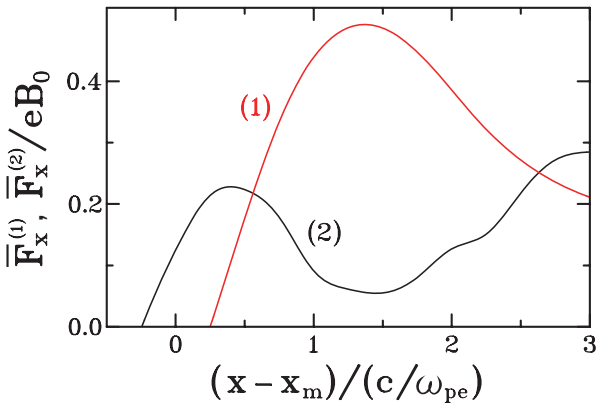

Fig. 7 Ion forces in the x direction at $\Omega_{i0}t = 0.9$ for the z-ranges (1) and (2) of Fig. 6.

958 and $26 < z/(c/\omega_{pe}) < 49$. The middle and lower panels show distributions of ions with $p_{ix} > 0.2 m_i c$ for the different range of z, $40 < z/(c/\omega_{pe}) < 44$ denoted by (1) and $31 < z/(c/\omega_{pe}) < 35$ denoted by (2). This clearly shows that the ion reflection in region (1) is strong, whereas that in region (2) is weak. Because the reflected ions tend to compress magnetic field [9], magnetic field lines bend forward in the region (1) compared to region (2). Further, because the reflected ions gain energies from the electromagnetic field, the ion reflection causes the damping of B_z [9]. Therefore, B_z is weaker in the region (1) than in the region (2) at $\Omega_{i0}t = 1.125$, which is slightly after the time when the ion reflection starts.

Figure 7 shows the forces on ions in the z-ranges (1) and (2) of Fig. 6 at $\Omega_{i0}t = 0.9$. This time is just before the time when the ion reflection starts. We define the averaged ion force as

$$\boldsymbol{F}(x,z) = q[\boldsymbol{E}(x,z) + \boldsymbol{u}(x,z) \times \boldsymbol{B}(x,z)/c], \tag{7}$$

where $\boldsymbol{u}$ is the ion fluid velocity,

$$\boldsymbol{u}(x,z) = \frac{\int \boldsymbol{v} f(x,z,\boldsymbol{v}) d\boldsymbol{v}}{\int f(x,z,\boldsymbol{v}) d\boldsymbol{v}}. \tag{8}$$

We write the x component of $\boldsymbol{F}$ averaged over the z-ranges (1) and (2) as $\bar{F}_x^{(1)}$ and $\bar{F}_x^{(2)}$, respectively. This figure clearly shows that in front of x_m, where x_m is the position at which $\bar{B}_z$ becomes maximum, $\bar{F}_x^{(1)}$ is much stronger than $\bar{F}_x^{(2)}$. This confirms that the strong ion reflection is caused by the strong ion force in the x direction, because the change in the position z of ions during the period from $\Omega_{i0}t = 0.9$ to 1.125 is negligibly small.

5. Summary

We have studied shock formation processes arising from the collision of exploding and surrounding plasmas with 2D electromagnetic particle simulations, for the case in which the initial velocity of the exploding plasma is perpendicular to an external magnetic field. As in the previous 1D simulations, a strong magnetic-field pulse is formed because of the penetration of the exploding ions, and the pulse reflects ions, generating forward and reverse shock waves. The 2D structure of the pulse and its effect on ion reflection were also investigated with attention to the evolution of whistler wave instabilities caused by relative cross-field motion between ions and electrons. Long-time evolution of 2D structures of forward and reverse shock waves is a future subject.

Acknowledgments

This work was carried out as part of the collaboration program under Grant No. NIFS12KNSS036 of the National Institute for Fusion Science, and of the joint research program of the Solar-Terrestrial Environment Laboratory, Nagoya University, and was supported in part by a Grant-in-Aid for Scientific Research (C) Grant No. 21540510 from the Japan Society for the Promotion of Science.

[1] Y. Ohsawa, Phys. Fluids **28**, 2130 (1985).
[2] T. Iwata, S. Takahashi and Y. Ohsawa, Phys. Plasmas **19**, 022302 (2012) and references therein.
[3] D.W. Forslund and C.R. Shonk, Phys. Rev. Lett. **25**, 1699 (1970).
[4] L. Spitzer, *Physical Processes in the Interstellar Medium* (Wiley-Interscience, New York, 1978).
[5] K. Yamauchi and Y. Ohsawa, Phys. Plasmas **14**, 053110 (2007).
[6] Y. Takeyama, S.-I. Nakayama and Y. Ohsawa, Phys. Plasmas **18**, 092307 (2011).
[7] J.B. McBride and E. Ott, Phys. Lett. A **39**, 363 (1972).
[8] J.B. McBride, E. Ott, J.P. Boris and J.H. Orens, Phys. Fluids **15**, 2367 (1972).
[9] T. Kawashima, S. Miyahara and Y. Ohsawa, J. Phys. Soc. Jpn. **72**, 1664 (2003).